DFT Study of the Monomers and Dimers of 2-Pyrrolidone: Equilibrium Structures, Vibrational, Orbital, Topological, and NBO Analysis of Hydrogen-Bonded Interactions

Andrew E. Shchavlev

Division of Computational and Informational Science, Volga Region Academy of State Service, 23/25 Sobornaya Street, Saratov 410031, Russia

Alexei N. Pankratov*

Department of Chemistry, N. G. Chernyshevskii Saratov State University, 83 Astrakhanskaya Street, Saratov 410012, Russia

Vladimir B. Borodulin and Olga A. Chaplygina

Department of Biological Chemistry, Saratov State Medicinal University, 112 Bol'shaya Kazach'ya Street, Saratov 410012, Russia

Received: July 8, 2005; In Final Form: September 29, 2005

A computational study of the monomers and hydrogen-bonded dimers of 2-pyrrolidone was executed at different DFT levels and basis sets. The above dimeric complexes were treated theoretically to elucidate the nature of the intermolecular hydrogen bonds, geometry, thermodynamic parameters, interaction energies, and charge transfer. The processes of dimer formation from monomers and concerted reactions of double proton transfer were considered. The evolution of geometry, vibrational frequencies, charge distribution, and AIM properties in going from monomers to dimers was systematically followed. The solvent effects upon dimer formation were investigated in terms of the self-consistent reaction field (SCRF Onsager model). For the monomers and three dimers, vibrational frequencies were calculated and the changes in frequencies of the vibrations most sensitive to complexation were discussed. The orbital interactions were shown to lengthen the X−H (X = N, O) bond and lower its vibrational frequency (a red shift). To better understand the nature of the corresponding intermolecular interactions, we performed natural bond orbital (NBO) analysis. Topological analysis of electron density at bond critical points (BCP) was executed for complex molecules using the Bader's atoms in molecules (AIM) theory. The interaction energies were calculated, and the basis set superposition errors (BSSE) were estimated systematically. Satisfactory correlations between the structural parameters, interaction energies, and electron density characteristics at BCP were found.

1. Introduction

Hydrogen bonding is the interaction that plays an important role in solvation,[1] supramolecular chemistry,[2] the secondary structure of proteins[3] and DNA,[4] atmospheric chemistry,[5] and so forth. Of all intermolecular interactions, hydrogen bonding, both proper and improper,[6−9] is of special interest because of its relevance to biochemical phenomena, molecular recognition, and organic synthesis. The molecules that constitute a complex are often bound with each other by means of hydrogen bonds. The studies of such molecular complexes (clusters) are of importance for understanding a wide variety of chemical and biochemical processes.[10,11]

2-Pyrrolidone (2-pyrrolidinone, pyrrolidine-2-one, 2-oxopyrrolidine, γ-butyrolactam) is a precursor of prospective drugs for the treatment of sea sickness, hypertension, and a number of different pathologies including cancer. A patent has been registered for a highly efficient and nontoxic pharmaceutical preparation containing lactams with 4−6 carbon atoms (including γ-butyrolactam) as the active ingredients.[12] 2-Pyrrolidone is also used widely as a ligand for the formation of biologically active complexes with platinum and palladium cations. Thus, in 1991 Shebaldova et al.[13] reported on the synthesis of a Pd(II) coordination compound with 2-pyrrolidone and chloride ion and on the determination of the molecular structure of the above complex exhibiting a high biological activity.

2-Pyrrolidone is capable of undergoing the lactam−lactim tautomerization. In particular, it is known that 2-pyrrolidone reacts with the palladium (II) cation in the lactim hydroxy form.[13]

The presence of electron-rich centers (N, O) and labile hydrogen atom offers the possibility of formation of intermolecular hydrogen bonds of different types: N−H···O, N−H···N, O−H···O, and O−H···N.

These bond types can generate different kinds of 2-pyrrolidone dimeric species, which are of fundamental interest to biochemistry. In particular, all hypothalamus hormones are low-molecular peptides, and many of them carry a fragment of pyroglutamic acid,[14] that is, in essence, the fragment of 2-pyrrolidone. Such hormones are thyroliberin, gonadoliberin, melanostatin, and so forth. The sites of synthesis of hypothalamus hormones are nerve endings, synaptosomes of the hypothalamus. The large amounts of hormone associates have just been discovered here. It cannot be excluded that the aforemen-

* Corresponding author. E-mail: pankratovan@chem.sgu.ru.

10.1021/jp053753m CCC: $30.25
Published on Web 11/09/2005

tioned associate species are stabilized by hydrogen bonds of the pyroglutamic acid fragment.

IR and Raman spectroscopic data along with the results of dielectric measurements in different solvents testify the existence of monomer−dimer equilibrium.[15−17] The structure of 2-pyrrolidone monomers has been explored extensively by various experimental[18] and theoretical[18−24] methods.

Differential scanning calorimetry revealed the presence of a previously unknown metastable phase of 2-pyrrolidone in the range of 173−303 K with a melting point of 286 K.[18] However, 2-pyrrolidone dimers were not studied satisfactorily. Therefore, fundamental studies are required to shed light on these interesting systems. In particular, the dynamics of the hydrogen bond system of 2-pyrrolidone dimers deserves special interest.

The above dimers represent an example of self-assembling structures, which underlines the importance of evaluations the hydrogen-bonding intermolecular interactions.[25]

In this study, we apply different methods of the density functional theory to gain deeper insight into the nature of the intermolecular interactions that bind the 2-pyrrolidone monomeric units in dimers.

In relation to the aforesaid, the aim of this work is the elucidation of the structure and properties of 2-pyrrolidone dimers using the contemporary quantum chemical approaches. The paper is organized as follows. The Computational Methods Section outlines the computational details. Sections 3.1 and 3.2 present the geometry and IR spectra for monomers and dimers. Section 3.3 displays the thermodynamic parameters and activation barriers, and Section 3.4 shows the Mulliken and natural population analysis (NPA) charge distribution and dipole moments. Section 3.5 outlines the orbital interactions of the studied compounds. In Section 3.6, the NBO and AIM analyses are considered. Section 3.7 presents hydrogen-bonded energies and BSSE corrections. Finally, the Concluding Remarks Section provides the general summary.

2. Computational Methods

All calculations were carried out using the Gaussian 98 series program[26] without any geometry restrictions. Three density functional methods were used: the hybrid B3LYP functional, which combines the three-parameter exchange functional by Becke[27] with the LYP correlation functional;[28] the hybrid model called the modified Perdew−Wang one-parameter model for kinetics (MPW1K);[29] the hybrid functional B3PW91, which contains the above Becke three-parameter exchange functional with a nonlocal correlation provided by the Perdew−Wang gradient-corrected functional.[30] The 6-311++G(d,p)[31,32] and AUG-cc-PVDZ[33,34] basis sets were used. Diffuse functions were included in order to treat the lone electron pairs properly. All equilibrium structures without the imaginary frequencies correspond to the minima points on the potential energy surfaces. The initial geometries were generated by means of HyperChem (HyperChem, Hypercube, Inc., Gainesville, FL 32601). Harmonic vibrational frequencies were computed to evaluate the zero-point vibrational energy (ZPVE) corrections, which we have included in all the relative energies. The transition state calculations were performed using the synchronous transit-guided quasi-Newton (STQN) method.[35] For characterizing the transition states, the existence of imaginary frequencies[36] was stated initially, and then the intrinsic reaction coordinate (IRC)[37] leading to the corresponding energy minima was calculated. The Onsager self-consistent reaction field (SCRF) method[38] at the MPW1K/6-311++G(d,p) level was applied to compute the molecular properties in solution.

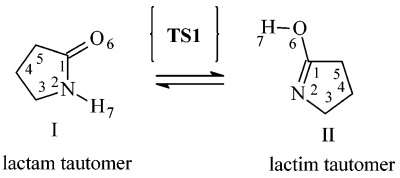

Figure 1. Structure and atom labeling for tautomers **I** and **II**.

Employing the notation of Xantheas,[39] the uncorrected interaction energies were obtained by subtracting the energy of fully optimized monomers from the energies of dimers

$$\Delta E = E^{ab}{}_{AB}(AB) - E^{a}{}_{A}(A) - E^{b}{}_{B}(B)$$

where the superscripts denote the basis set and the subscripts denote the geometry used for the energy calculations.

The BSSE quantity was obtained using the Boys−Bernardi method:[40]

$$BSSE = [E^{ab}{}_{AB}(A) + E^{ab}{}_{AB}(B)] - [E^{a}{}_{A}(A) + E^{b}{}_{B}(B)]$$

To better understand the nature of the intermolecular interactions, we performed natural bond orbital (NBO) analysis with the NBO 3.1 program.[41]

To describe the electronic structure of 2-pyrrolidone, we performed the topological analysis by means of Bader's atoms in molecules (AIM) theory[42,43] at the B3LYP/6-311++G(d,p) level to calculate the charge density (ρ) and the Laplacian of the charge density ($\nabla^2\rho$). The AIM calculations were carried out using the critical point option for the AIM keyword.

The vibrational frequencies were computed for the optimized geometries of monomers and dimers of 2-pyrrolidone at different levels of theory and basis sets. The harmonic frequency shift of the O−H stretching mode in the dimers, $\Delta\nu_{0-H}$, was estimated by the following equation:

$$\Delta\nu_{0-H} = \nu_{0-H(complex)} - \nu_{0-H(monomer)}$$

To improve the frequency shift estimation, we calculated the corresponding scale factors using the technique proposed in refs 44 and 45. The optimal scale factors were defined from the ratio ν^{exptl}/ν^{calcd}. The predicted frequency shift was determined as follows

$$\Delta\nu^{scal} = k_i(\nu_{complex} - \nu_{monomer})$$

where k_i is the corresponding "optimal" scale factor.

3. Results and Discussion

3.1. Geometry Parameters of Monomers and Dimers. The most important geometry parameters of the monomers and dimers of 2-pyrrolidone (Figure 1) are given in Table 1. The analysis of the harmonic vibrational frequencies at all DFT theory levels showed that all of the structures obtained are minima (imaginary frequencies are absent).

The molecular systems of monomers and the transition state originated from their mutual transformations belong to the C_1 point group. Results deduced from X-ray analysis[18] and optimized geometries of molecule **I** are compared in Table 1. The monomer **I** geometry optimized by means of different DFT levels is very close to the experimental one. Somewhat distinct are the optimized and experimental geometries of the carbonyl group. The C═O bond in crystal is longer compared to the calculated one. The C1−N2 distance in crystal is 0.035 Å shorter and C1−O6 (C═O) is 0.023 Å longer than the corresponding

TABLE 1: Selected Geometries for Monomers and Dimers of 2-Pyrrolidone Optimized at Different Theory Levels[a]

	B3LYP		MPW1K		B3PW91		
parameter	6-311++G(d,p)	AUG-cc-pVDZ	6-311++G(d,p)	AUG-cc-pVDZ	6-311++G(d,p)	AUG-cc-pVDZ	exptl[18]
			monomer **I**				
C1−N2	1.370	1.372	1.356	1.357	1.367	1.368	1.335
C1−O6	1.215	1.221	1.202	1.208	1.213	1.219	1.238
N2−H7	1.009	1.011	1.001	1.003	1.008	1.010	
C1−C5	1.530	1.530	1.513	1.514	1.525	1.525	1.518
C3−N2	1.457	1.458	1.440	1.441	1.451	1.451	1.460
<N2−C1−O6>	125.975	125.783	125.996	125.806	125.984	125.788	125.90
<C1−N2−H7>	119.940	119.873	119.907	119.791	119.937	119.893	
			monomer **II**				
C1−N2	1.269	1.274	1.258	1.263	1.269	1.274	
C1−O6	1.348	1.352	1.329	1.333	1.342	1.346	
O6−H7	0.968	0.970	0.957	0.959	0.967	0.969	
C1−C5	1.507	1.508	1.494	1.495	1.503	1.503	
C3−N2	1.471	1.472	1.452	1.453	1.463	1.464	
<N2−C1−O6>	123.832	123.721	123.837	123.748	123.715	123.629	
<C1−O6−H7>	107.215	107.093	107.324	107.755	106.854	106.707	
<N2−C1−O6−H7>	0.569	0.527	0.625	0.590	0.602	0.536	
			dimer **III**				
C1−N2	1.350	1.351	1.336	1.338	1.346	1.347	
C1−O6	1.232	1.238	1.218	1.224	1.230	1.236	
N2−H7	1.027	1.032	1.020	1.024	1.029	1.034	
C1−C5	1.527	1.527	1.510	1.511	1.521	1.521	
C3−N2	1.458	1.459	1.441	1.442	1.451	1.452	
O6−H14	1.869	1.831	1.836	1.805	1.843	1.804	
N2−O13	2.889	2.858	2.849	2.825	2.866	2.834	2.922
<N2−C1−O6>	126.263	126.145	126.280	126.157	126.624	126.150	
<C1−N2−H7>	121.092	121.221	121.090	121.213	121.123	121.276	
<C1−O6−H14>	120.683	118.846	120.707	118.666	120.082	118.117	
<O6−H14−N8>	171.771	173.624	171.731	173.762	172.224	174.280	172.3
<C1−O6−H14−N1>	2.271	3.634	2.077	3.545	1.872	3.758	
			dimer **IV**				
C1−N2	1.290	1.295	1.278	1.282	1.294	1.298	
C1−O6	1.311	1.313	1.294	1.298	1.297	1.299	
O6−H14	1.036	1.044	1.024	1.029	1.074	1.081	
C1−C5	1.511	1.513	1.497	1.498	1.508	1.510	
C3−N2	1.471	1.470	1.452	1.453	1.462	1.461	
H14−N8	1.599	1.573	1.577	1.563	1.482	1.469	
N2−O13	2.636	2.617	2.600	2.592	2.556	2.544	
<N2−C1−O6>	125.610	125.531	125.608	125.485	125.625	125.531	
<C1−O6−H14>	111.279	111.337	111.066	110.971	111.324	111.453	
<O6−H14−N8>	178.772	179.171	178.616	179.234	178.774	179.119	
<C1−O6−H14−N8>	4.054	6.259	3.516	5.503	6.704	7.701	
			dimer **V**				
C1−N2	1.344	1.346	1.331	1.333	1.340	1.342	
C1−O6	1.235	1.242	1.222	1.228	1.234	1.241	
N2−H7	1.034	1.038	1.027	1.029	1.038	1.042	
C1−C5	1.524	1.524	1.507	1.508	1.518	1.518	
C3−N2	1.458	1.459	1.441	1.442	1.450	1.452	
O6−H14	1.664	1.639	1.631	1.618	1.628	1.609	
H14−O13	1.001	1.007	0.990	0.995	1.005	1.011	
H7−N8	1.914	1.879	1.872	1.853	1.862	1.833	
N8−C9	1.284	1.289	1.273	1.277	1.284	1.289	
C9−O13	1.321	1.324	1.304	1.307	1.314	1.317	
C9−C10	1.512	1.513	1.497	1.499	1.507	1.508	
N8−C12	1.471	1.471	1.453	1.454	1.463	1.464	
O6−O13	2.662	2.641	2.621	2.609	2.630	2.614	
N2−N8	2.923	2.923	2.875	2.862	2.877	2.865	
<N2−C1−O6>	125.938	125.837	125.919	125.834	125.921	125.828	
<C1−O6−H14>	123.163	121.656	123.520	121.998	122.616	121.146	
<O6−H14−O13>	174.544	173.309	174.979	173.562	174.186	172.944	
<C1−N2−H7>	119.592	119.723	119.369	119.519	119.419	119.579	
<N2−H7−N8>	164.446	165.782	164.403	165.642	165.085	166.329	
<C9−O13−H14>	112.664	112.817	112.691	112.770	112.552	112.682	

[a] Bond lengths in Å, angles in degrees.

computed distances in monomer **I**. In general, the bond lengths and valence angles in **I** are close to the corresponding computed quantities offered by different methods. All of the molecules show a distinctly nonplanar configuration. The consideration of bond distances and angles of the ring demonstrates that the ring is unstrained.[18] Indeed, monomer **I** adopts a form similar to an unstrained envelope with the fold running from C3 to C5 and C4 at the apex. The rest molecule C3−N2−C1(O6)−C5

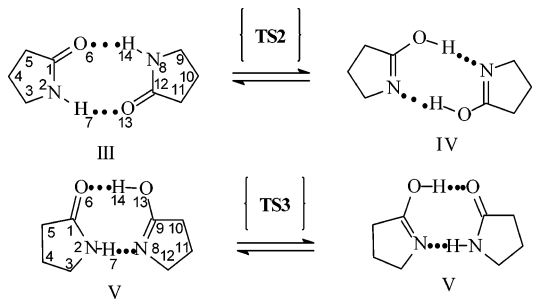

Figure 2. Theoretically assumed dimers **III**−**V**.

has an approximately planar character. Calculations for **I** reveal a slight pyramidalization of the N atom; thus, the lone pair and the apex atom, C4, appear at the same side of the C3−N2−C1(O6)−C5 fragment. The pyramidalization is reduced on hydrogen bonding in the studied dimers.

In the case of lactim tautomer **II**, the C1−O6 bond is ordinary single, and, naturally, longer compared to the C1−O6 double bond in lactam **I**. In contrast, the N1−C2 distance in **II** (C═N bond) is shorter than that in **I** (C−N). In general, structure **II** represents an unstrained envelope with C4 at the apex. However, the C1−C2−C3−C4 dihedral angle is opposite in sign, although close by absolute value compared to monomer **I**.

The comparison between the geometry parameters of the monomers and dimers (Figure 2) shows that the association of two monomeric molecules into a dimer causes substantial changes in the bond lengths and angles. These discernible differences are due to the effect of hydrogen bonding between the O, N, and H atoms of the monomeric species. Dimers **III** and **IV** may exist in two forms with C_i and C_2 symmetry, respectively, with an inversion center, and dimer **V** has a C_1 symmetry point group. Species **III**−**V** are found to have a nonplanar backbone structure (envelope conformation of each monomeric unit). It appeared that each of the dimers of **III** and **IV** is composed of two monomers with identical geometries. That is why Table 1 contains the structural parameters of a single monomer for every aforesaid dimer.

Let us discuss dimers **III** and **IV** entering the C_i and C_2 symmetry point groups. B3LYP/6-311++G(d,p) calculations show that the C_i and C_2 structures have essentially the same spatial and energetic characteristics; it is also valid for the transition states of dimers interconversion reactions. For example, the difference between the total energies of the C_i and C_2 structures (dimer **III**) represents a very small value of ∼0.004 kcal/mol. That is comparable to the heat molecular journey. Therefore, all of the further discussion and Tables imply C_i structures of dimers **III** and **IV**.

Among all of the studied dimers, molecule **III** is the most stable. The experiment[18] shows that this complex crystallizes in the form of centrosymmetric species. The geometry studies reveal the presence of hydrogen-bonding interactions between two equivalent O···H−N hydrogen bonds, with an O···H distance of 1.869 Å (B3LYP/6-311++(d,p)) or 1.836 Å (MPW1K/6-311++(d,p)). Hydrogen-bond formation results in an N−H bond elongation of ∼0.018 Å (B3LYP/6-311++(d,p)). The N···O distance of 2.889 Å (B3LYP/6-311++(d,p)) agrees with the X-ray experimental value of 2.992 Å.[18] The arrangement of atoms, hydrogen-bond participants, has been established to be about linear (<O6−H14−N8> = 172−174°).

The second place by stability is occupied by dimer **V**. In this structure, the distances between the nearest atoms of 2-pyrrolidone monomers (B3LYP/6-311++(d,p)) are 1.664 Å (O···H−O) and 1.914 Å (N···H−N). According to different theory levels, the O6−H14−O13 angle in **V** is 173−175° and the N2−H7−N8 angle is 164−166°.

Dimer **IV** possesses two hydrogen bonds, N···H−O with lengths of 1.599 Å (B3LYP/6-311++(d,p)). The <O6−H14−N8> angle is 178−179°, confirming a practically linear arrangement.

The data as a whole indicate that dimers **III**, **IV**, and **V** are hydrogen-bonded clusters. As a result of the geometric restrictions in **III**−**V**, the optimized geometries showed marked deviations from the idealized 180° for the following dihedral angles: in dimer **III** <C1−O6−H14−N8 = 2.271°; in dimer **IV** <C1−O6−H14−N8 = 4.054°; in dimer **V** <C1−O6−H14−O13 = −173.403°, <N2−H7−N8−C9 = 2.139° (B3LYP/6-311++G(d,p) level of theory). A slight deviation from the energetically most favorable linear arrangement of the X−H···Y fragment (X, Y = N, O) indicates a relatively strong hydrogen-bonded interaction.

As can be seen from Table 1, the O−H bonds of the proton-donating moiety are elongated on complexation compared to monomer **II** (by ∼0.060 Å in dimer **IV** and ∼0.030 Å in dimer **V** almost at all the theory levels), that is accompanied by a C−O bond contraction by ∼0.040 Å (**IV**) and by ∼0.100 Å (**V**). An exception is the elongation value for the O−H bond in **IV** versus **II**, which is equal to 0.107 Å according to the B3PW91 data.

The N−H bond length also increases by ∼0.020 Å (dimer **III**) and by ∼0.030 Å (dimer **V**) at all of the theory levels compared to monomer **I**. Therewith, the C═O bond in dimer **III** lengthens by ∼0.020 Å.

The X−H (X = N, O) bond elongation may be a result of electrostatic interactions, charge redistributions, and orbital interactions.[9]

The contraction by about 0.25 Å of the O···N intermolecular distance is observed on going from dimer **III** to dimer **IV**. The combinations of exchange and correlation functionals in the B3LYP and B3PW91 methods yield very similar geometry parameters for located global minima on the corresponding potential energy surfaces. The geometry parameters obtained with the 6-311++G(d,p) and AUG-cc-pVDZ basis sets within the same method are also comparable. More strict evaluation of the O···H−N, N···H−O, O···H−O, and N···H−N intermolecular hydrogen bonds in the dimers will be presented below on the basis of the calculated hydrogen-bonded interaction energies, as well as NBO analysis and AIM electron density at bond critical points.

3.2. Vibrational Analysis. The vibrational frequencies of monomers **I**, **II**, and dimers **III**−**V** of 2-pyrrolidone were obtained in the present work from the DFT calculation and were compared with the relevant experimental data[46] in Table 2. The calculated stretching vibration frequencies of monomer **I** deviate from the experimental frequencies for the reasons discussed in refs 47 and 48.

When passing from 2-pyrrolidone monomers to dimers, changes in the vibrational spectra were observed, which confirm the conclusions made on the basis of the calculated hydrogen-bonding energies (Section 3.7). Table 2 displays the computed changes ($\Delta\nu^{scal}$) in the vibrational frequencies most sensitive to aggregation in moving from monomers to dimers. As seen from Table 2, the negative shifts in dimer **III** caused by the N−H and C═O group participation in hydrogen bonds (two O···H bonds) adopt the following values: $\Delta\nu$(N−H) = 286−372 cm^{-1} and $\Delta\nu$(C═O) = 28−32 cm^{-1}. In dimer **IV**, the calculated negative shifts $\Delta\nu$(O−H) are much higher: 1199−

TABLE 2: Selected Calculated Stretching Vibrational Frequencies (cm^{-1}) and Changes ($\Delta\nu$) in the IR Frequencies from 2-Pyrrolidone Monomers to Dimers III−V

	B3LYP		MPW1K		B3PW91		MPW1K (in solution)[a]	
parameter	6-311++G(d,p)	AUG-cc-pVDZ	6-311++G(d,p)	AUG-cc-pVDZ	6-311++G(d,p)	AUG-cc-pVDZ	6-311++G(d,p)	exptl[46]
				monomer **I**				
ν(N−H)	3627	3621	3754	3750	3650	3644	3755	3474
ν(C═O)	1786	1777	1886	1874	1809	1800	1845	1757
				monomer **II**				
ν(O−H)	3764	3748	3937	3920	3794	3774	3942	
				dimer **III**				
ν(N−H)	3328	3280	3437	3395	3309	3254	3423	
$\Delta\nu^{scal}$N−H)	−286	−327	−293	−329	−324	−372	−332	
ν(C═O)	1755	1749	1851	1841	1778	1770	1833	
$\Delta\nu^{scal}$(C═O)	−30	−28	−32	−31	−30	−29	−11	
				dimer **IV**				
ν(O−H)	2564	2445	2681	2604	2053	2010	2623	
$\Delta\nu$(O−H)	−1199	−1303	−1256	−1316	−1740	−1764	−1318	
				dimer **V**				
ν(N−H)	3199	3147	3298	3263	3135	3085	3289	
$\Delta\nu^{scal}$(N−H)	−410	−455	−422	−451	−490	−533	−431	
ν(C═O)	1742	1737	1835	1827	1762	1756	1817	
$\Delta\nu^{scal}$(C═O)	−43	−39	−47	−44	−45	−43	−26	
ν(O−H)	3096	3012	3213	3151	3017	2934	3183	
$\Delta\nu$(O−H)	−668	−736	−724	−769	−777	−840	−759	

[a] SCRF Onsager method (the solvent is water).

1764 cm^{-1}. It is interesting that for dimer **IV** the above shifts are not large except for the ν(O−H) stretching mode. That is in marked contrast to dimer **V**, in which $\Delta\nu$(C═O) = 43−47 cm^{-1}, $\Delta\nu$(N−H) = 410−533 cm^{-1}, and $\Delta\nu$(O−H) = 668−840 cm^{-1}. Among all of the features of vibrations, the ν(O−H) stretching mode for dimer **IV** occurs at discernibly lower frequencies compared to the monomer, than in the corresponding monomer, and the calculated frequencies point to the presence of a relatively strong N···H−O interaction in dimer **IV**. The higher vibrational shifts obtained for dimer **IV** provide additional evidence for the substantial hydrogen bonds cooperativity in structure **IV**. It should be useful to note that in the aqueous solution (SCRF Onsager method) $\Delta\nu$(C═O) becomes smaller (dimers **III** and **V**) and $\Delta\nu$(O−H) becomes greater (dimers **IV** and **V**) compared to the gaseous-phase calculations.

For all of the dimers with "proper" hydrogen bonding, the elongation of X−H bonds resulting in a downshift of stretching vibrational frequencies takes place.[45] For the downshift (red-shift) hydrogen bonds, there is additional bond lengthening because of orbital interactions that is not overcome by the moderate bond compression resulting from the repulsive interactions.[45]

The plot of X−H vibrational frequencies against X−H bond lengths shows the symbate behavior of the aforementioned values (Figure 3). Therefore, red-shift means X−H elongation and vice versa.

3.3. Thermodynamic Parameters and Activation Energies. The results of the gaseous-phase calculations (Table 3) of two feasible monomers (**I** and **II**) using the different DFT methods and basis sets indicate that the more stable structure is **I**. Monomer **II** is 12−13 kcal/mol less stable than **I**. These results show that in the gaseous phase lactam tautomer **I** should exist solely. The latter statement is confirmed by the experimental data on heat of formation,[49] IR spectrum,[46] and dipole moment.[15−17,50] The **I** → **II** proton-transfer reaction and the reverse process have been studied in this paper. The above transfer in 2-pyrrolidone may occur because of a short distance (about 2.6 Å) between O and H. The transition state of tautomerization (referred to as **TS1**) was computed, and the existence of a first-order saddle point was proved. Table 4 contains the calculated gaseous-phase energy differences between the **TS1** transition structure and stable tautomers **I** and **II**. The values of **I** → **II** barriers calculated using the B3LYP, MPW1K, and B3PW91 methods with different basis sets are within the range of 46−52 kcal/mol. The reverse reaction **II** → **I** barrier has values of 33−38 kcal/mol. As a reference method for the most precise computations of the transition states, MPW1K was chosen, which simulates both the geometry of saddle point structures and the barrier heights quite adequately.[51] As is seen, both barriers are too high, and the proton transfer from **I** to **II** and from **II** to **I** is difficult to be observed experimentally in the gaseous phase. To study the relative stability of the above tautomers in aqueous solution, we considered the solvation effect using the SCRF method, which is based on Onsager's reaction field theory. The solvent effect is given in Table 3, where the energies of the solvated species in water (dielectric constant ϵ = 78.39) are presented. It can be inferred from this Table that the stability order of the forms does not depend on solvation effect. Monomer **I** also predominates in aqueous solution. The barrier height for the **I** → **II** reaction in aqueous solution is essentially the same as that for the gaseous phase, and the barrier height for the reverse process decreases by 2.292 kcal/mol (MPW1K/6-311++G(d,p)). In connection with the aforesaid, the **I** ⇄ **II** intramolecular

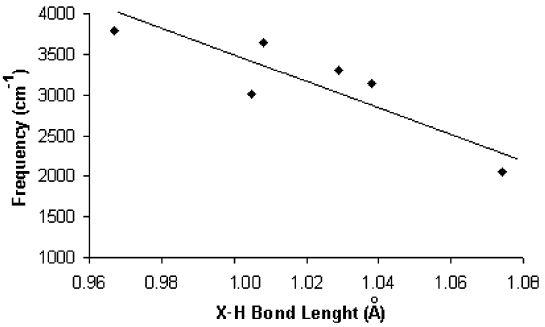

Figure 3. Relationship between stretching vibrational frequencies and bond lengths for X−H (B3PW91/6-311++G(d,p)).

TABLE 3: Total[a] *E* (au) and Δ*E* (kcal/mol) Relative to Monomer I for the Monomers and Total[a] *E* (au) and Δ*E* (kcal/mol) Relative to Dimer III for the Dimers of 2-Pyrrolidone in the Gaseous Phase and in Aqueous Solution at Different Theory Levels Including Zero-Point Energy Correction

	B3LYP		MPW1K			B3PW91	
	6-311++G(d,p)	AUG-cc-pVDZ	6-311++G(d,p)	AUG-cc-pVDZ	6-311++G(d,p) (in solution[b])	6-311++G(d,p)	AUG-cc-pVDZ
monomer **I**	−286.603102	−286.556214	−286.507492	−286.469446	−286.512074	−286.493223	−286.451649
monomer **II**	−286.581342	−286.535824	−286.485409	−286.448800	−286.486012	−286.471225	−286.431081
Δ*E*(**II**−**I**)	13.655	12.795	13.857	12.955	16.354	13.804	12.907
dimer **III**	−573.225061	−573.132261	−573.035375	−572.959866	−573.035498	−573.004621	−572.922305
dimer **IV**	−573.195299	−573.105679	−573.007323	−572.933330	−573.007527	−572.979738	−572.896377
Δ*E*(**IV**−**III**)	18.676	16.680	17.603	16.651	17.552	15.614	16.270
dimer **V**	−573.206664	−573.114979	−573.017224	−572.942288	−573.019345	−572.986854	−572.905573
Δ*E*(**V**−**III**)	11.544	10.845	11.389	11.030	10.136	11.149	10.499

[a] Sum of electronic and thermal energies. [b] SCRF Onsager method (the solvent is water).

TABLE 4: Intramolecular Proton Transfer Activation Energies for the Monomers and Intermolecular Double Proton Transfer Activation Energies for the Dimers of 2-Pyrrolidone in the Gaseous Phase and in Aqueous Solution Including Zero-Point Corrections (kcal/mol)

	B3LYP		MPW1K		B3PW91	
process and transition state	6-311++G(d,p)	AUG-cc-pVDZ	6-311++G(d,p)	AUG-cc-pVDZ	6-311++G(d,p)	AUG-cc-pVDZ
TS1 (monomer): **I** → **II**	48.832	48.321	52.255	50.695	48.318	46.785
TS1 (monomer): **II** → **I**	36.178	35.526	38.398	37.739	34.514	33.878
TS1 (monomer): **I** → **II**			52.646			
TS1 (monomer): **II** → **I** (in solution)[a]			36.292			
TS2 (dimer): **III** → **IV**	15.251	13.938	14.608	13.688	13.348	12.921
TS2 (dimer): **IV** → **III**	−2.833	−2.742	−2.994	−2.963	−2.265	−2.245
TS2 (dimer): **III** → **IV**			14.379			
TS2 (dimer): **IV** → **III** (in solution)			−3.173			
TS3 (dimer): **V** → **V**	3.734	2.978	3.396	2.915	2.199	1.653
TS3 (dimer): **V** → **V** (in solution)			3.104			

[a] SCRF Onsager method (the solvent is water).

tautomerization reaction is a quite disfavored process or not a spontaneous process in both the gaseous phase and aqueous medium.

Table 3 contains the total and relative energies of 2-pyrrolidone dimers **III**, **IV**, and **V**. The relative energies are corrected for ZPVE differences. It can be seen that, regardless to the DFT methods and basis set used, dimer **III** is more stable than **IV** and **V** in the gaseous phase. The difference in energy between **III** and **IV** decreases by a 2.5 kcal/mol in going from the B3LYP to B3PW91 method of computations. Using the AUG-cc-pVDZ basis set, we repeated the DFT calculations and found approximately the same energies and relative stabilities as with the 6-311++G(d,p) basis set.

The reactions of double proton transfer **III** → **IV** and **V** → **V** have been considered in this paper. A short distance between N and H (∼2 Å) serves as a prerequisite for the occurrence of these reactions. The transition states (**TS2** and **TS3**) for intermolecular double proton transfer were calculated, and the existence of first-order saddle points was confirmed. **TS2** and **TS3** possess nonplanar structures such as dimers **III**, **IV**, and **V**. It is seen easily from the **TS2** structure that the H7 proton attached initially to O6 then transfers to N8, and simultaneously the second proton H14 moves from O13 to N2. In the **TS3** transition structure, the H7 proton attached to N2 transfers to N8 and simultaneously the second proton H14 moves from O13 to O6. To clear up the question about whether any high-energy intermediate exists along the reaction path, we have computed the energetic profiles (intrinsic reaction coordinate) for double proton transfers at the B3LYP/6-311++G(d,p) level starting from transition states **TS2** and **TS3**. There are no intermediates along the intrinsic reaction coordinate, and the reactions proceed smoothly from reactant to product. It is safe to say in this connection that two protons in the gaseous phase transfer concertedly and synchronously.

The reaction **III** → **IV** barrier is ∼15 kcal/mol, and the reverse proton-transfer barrier accepts the value of ca. −3 kcal/mol. The latter means that the first vibrational level in the minimum is higher than the activation barrier. Obviously, the reverse proton-transfer reaction will proceed quickly. The **III** → **IV** reaction is endothermic, and the transition state geometry is close to that of the product according to the Hammond postulate.

In the case of the **V** → **V** process, the barrier height is ∼3.5 kcal/mol. Evidently, because of a low barrier the above proton transfer would proceed readily. The barriers heights for processes **III** → **IV**, **IV** → **III**, and **V** → **V** do not depend significantly on the theory level.

To show the solvation effect, we have also theoretically considered the above reactions in aqueous solution (via the SCRF Onsager method). Dimer **III** also predominates in aqueous solution. Similar to the double proton transfer, the heights of the reaction **III** → **IV**, **IV** → **III**, and **V** → **V** barriers remain practically unchanged in the aqueous medium compared to the gaseous phase.

3.4. Population and Dipole Moment Analysis of the Monomers and Dimers. The charge distributions calculated by the Mulliken and NBO methods for monomers **I** and **II** are given in Table 5. Both methods predict the same tendencies, assigning a positive partial charge of similar magnitudes on hydrogen atom H7, whereas there were greater variations between the methods in the magnitude of the partial charges on the oxygen, nitrogen, and carbon atoms. The NBO population

TABLE 5: Selected Mulliken and NPA Charges (q_i) of 2-Pyrrolidone Monomers and Charge Shifts (Δq_i) on Dimerization in the Gaseous Phase at the B3LYP/6-311++G(d,p) Theory Level

	monomer **I**		monomer **II**		dimer **III**		dimer **IV**		dimer **V**	
atom	Mulliken q_i	NPA q_i	Mulliken q_i	NPA q_i	Mulliken $\Delta q_i{}^a$ (e)	NPA $\Delta q_i{}^a$ (e)	Mulliken $\Delta q_i{}^a$ (e)	NPA $\Delta q_i{}^a$ (e)	Mulliken $\Delta q_i{}^a$ (e)	NPA $\Delta q_i{}^a$ (e)
C1	0.137	0.686	0.183	0.582	0.051	0.007	−0.058	0.063	−0.012	0.013
C3	−0.288	−0.169	−0.412	−0.192	−0.033	0.004	0.090	0.016	−0.066	0.003
C4	−0.309	−0.391	−0.199	−0.401	−0.028	−0.001	−0.118	0.002	−0.011	−0.001
C5	−0.264	−0.472	−0.424	−0.458	−0.095	0.007	0.039	0.004	−0.115	0.008
N2	−0.174	−0.652	−0.171	−0.551	−0.029	0.003	−0.157	−0.086	−0.014	0.001
O6	−0.372	−0.624	−0.212	−0.679	−0.031	−0.062	−0.167	−0.020	−0.058	−0.063
H7	0.296	0.398	0.296	0.482	0.153	0.046	0.344	0.020	0.299	0.049
C9									−0.104	0.041
C10									0.054	0.003
C11									−0.089	0.001
C12									0.032	0.011
N8									0.018	−0.073
O13									−0.131	−0.012
H14									0.166	0.031

[a] $\Delta q_i = q_i^{\text{complex}} - q_i^{\text{monomer}}$ (complex = dimer **III**, **IV**, or **V**; monomer = **I** or **II**).

TABLE 6: Dipole Moments (D) for Different Forms of 2-Pyrrolidone in the Gaseous Phase

	B3LYP		MPW1K		B3PW91		exptl
	6-311++G(d,p)	AUG-cc-pVDZ	6-311++G(d,p)	AUG-cc-pVDZ	6-311++G(d,p)	AUG-cc-pVDZ	
monomer **I**	4.309	4.039	4.366	4.326	4.309	4.266	3.74[a]; 3.79[b]; 3.80[c]; 3.91[d]; 3.96[e]
monomer **II**	1.384	1.343	1.389	1.342	1.353	1.314	
dimer **III** (C_i)	0.004	0.002	0.003	0.002	0.011	0.002	1.64[a]; 2.06[d]; 2.30[d]
dimer **III** (C_2)	0.159		0.178		0.155		
dimer **IV** (C_i)	0.001	0.000	0.001	0.000	0.005	0.000	
dimer **IV** (C_2)	0.144		0.166		0.143		
dimer **V** (C_1)	3.798	3.838	3.921	3.787	3.901	3.763	

[a] Measured in carbon tetrachloride by the second Debye method.[15] [b] Measured in 1,4-dioxane by the second Debye method.[50] [c] Measured in 1,4-dioxane by the second Debye method.[15] [d] Measured in benzene by the second Debye method.[16] [e] Obtained from linear and nonlinear dielectric data in benzene.[17]

analysis indicates highly negatively charged nitrogen and oxygen atoms. The value of nitrogen negative charge is reduced and the negative value of oxygen charge is increased passing from monomer **I** to **II**.

Different electronic charge distributions for tautomers **I** and **II** are also manifested in different values of their dipole moments (Table 6). The computed values are around 4.266−4.309 D for lactam tautomer **I** and 1.314−1.384 D for lactim tautomer **II**. The experimental dipole moment of 2-pyrrolidone is 3.80 D in 1,4-dioxane,[15] 3.91 D in benzene,[16] and 3.96 D in benzene.[17] Monomer **I**, because of its higher dipole moment, exhibits a more polar character and, therefore, has a greater affinity to polar solvent. Thus, in polar solvent structure **I** is expected to be stabilized to a greater extent than the hydroxy form, **II**, which has been confirmed by the thermodynamic data. According to the MPW1K/6-311++G(d,p) results, the stabilization effect for tautomer **I** in water with respect to the gaseous phase is equal to 2.873 kcal/mol, whereas for structure **II** the aforesaid value is 0.378 kcal/mol.

It would be interesting to consider the changes in charge distribution on dimerization. The Mulliken and natural population analyses were used to investigate the charge changes related to the driving forces of hydrogen-bond formation in dimers **III**−**V**. The calculated changes in charge distribution for all of the dimers are presented in Table 5. The significant changes are observed for the atoms, which take part in linking the two monomeric molecules together by hydrogen bonding.

For all of the dimers, one can observe the increase in positive charges on labile hydrogens, and the increase in the absolute values of negative charges on heteroatoms compared to the monomers. The exclusion is the N atom, a participant of N−H bond (dimers **III** and **IV**). The strength of an intermolecular hydrogen bond depends greatly on a donor basic group so that the more positive (less negative) is the charge on the atom with the lone pair and the poorer is the donor ability of the atom. As a whole, the results obtained testify to the fact that the considerable charge transfer occurs in all dimers, which suggests the strong orbital interactions (Section 3.5) leading to the X−H bond elongation (Section 3.1). In dimer **IV**, the charge transfer is exhibited to a considerably greater extent than for **III** and **V**, which, according to the just aforesaid, points to the stronger orbital interactions leading to the greater bond elongation.

Special attention must be given (Table 6) to the unsatisfactory agreement of the computed values of the dipole moment of dimer **III** compared to the experimental ones. Taking into account a high symmetry (C_i and C_2 point groups) of molecule **III**, the mutual compensation (to a considerable extent) of the bonds' dipole moments seem to be rather obvious, that is, the low computed values of dipole moments are apparently correct. Possibly, in the given case we come up against the error of experimental evaluations.

It should be mentioned that the calculated dipole moment of dimer **V** is much higher than that for dimers **III** and **IV**. Hence, the reaction field should exert a greater effect on structure **V**.

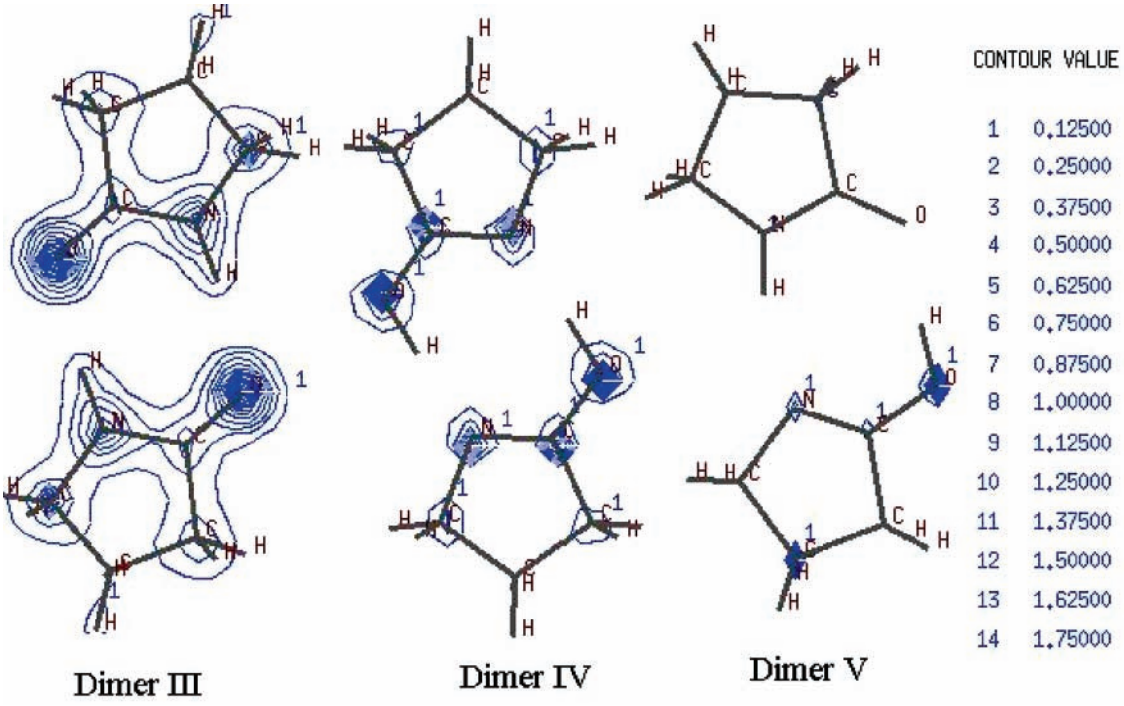

Figure 4. Contour map of the normal electron density for dimers **III**−**V** at B3LYP/6-311++G(d,p). The contour values in au are presented.

Such a suggestion has been supported by the energy evaluations. Thus, the stabilization effect of the aqueous medium in relation to the gaseous phase is 0.075, 0.128, and 4.458 kcal/mol for dimers **III**, **IV**, and **V**, respectively.

Figure 4 presents the normal electron density distribution for dimers **III**−**V**. Because the charge-controlled donor−acceptor interaction usually occurs more readily between one atom with explicit electron density and another atom with a small electron density, the most pronounced binding, in the case of reaction charge control,[50] would take place in **IV**, which agrees with the data (Section 3.3) on the greater interaction energy in dimer **IV** compared to **III** and **V**.

Moreover, the electrostatic potential distributions (Figure 5) show that for dimers **III**−**V** there are attractive electrostatic forces that draw together the monomeric units. Thus, the electrostatic attraction contributes to the overall interaction.

3.5. Orbital Interactions. The structural similarity of monomers **I** and **II** allows for the direct comparison between the orbital energies of these compounds. Figure 6 shows the energies and shapes of frontier orbitals 23 and 24 for monomers **I** and **II**. In monomer **I**, HOMO is higher and LUMO is lower compared to the corresponding orbitals of monomer **II**. Therewith, the HOMO energy changes to a greater extent than the LUMO energy. We have found that the proton movement from nitrogen to oxygen causes the HOMO energy to decrease by 0.009 au. It is interesting that the frontier orbitals of transition state **TS1** are closer in energy to monomer **I** than to **II**.

One can conclude from Figure 6 that HOMOs for dimers **III**−**V** are localized on all monomeric units, whereas the LUMOs for dimers **III** and **IV** are not localized on any monomeric unit, and the LUMO of dimer **V** is localized mainly on monomeric unit **I**. The energy differences of the corresponding (HOMO or LUMO) frontier orbitals between dimers **III**−**V** are neglected.

The charge transfer can be understood in terms of the frontier orbitals, that is, from the viewpoint of mixing of the one monomer's LUMO with the another monomer's HOMO. In the case of a simple hydrogen bond, a collinear geometry of Y···H−X yields a maximal overlap of HOMO (n_Y) and LUMO (σ^*_{H-X}), but because the local spherical symmetry of LUMO (it is mostly $1s_H$), collinearity is not a strict condition.[53]

Within the framework of this simplified approach, mixing the lone pair (HOMO to a great extent) of the proton acceptor with the X−H antibonding orbital (LUMO to a significant extent) of the proton donor is considered. NBO analysis (Section 3.6) indicates that this is the dominant interaction.

In principle, the X−H bond may also be present in HOMO. In the course of mixing the X−H bonding orbital with some proton acceptor orbital (which probably contributes to LUMO), the electron density would be lost from the X−H basin, that being accompanied by the X−H bond elongation.

Independent of the direction of electron density transfer, it is evident that the HOMO−LUMO interactions contribute to the elongation of the X−H bonds and the red shift of vibrational bands for dimers **III**−**V**.

Irrespective of the direction of electron density transfer, it is evident that the HOMO−LUMO interactions contribute to the X−H bonds elongation and to the bands' red shift in the vibrational spectra of dimers **III**−**V**.

3.6. NBO Analysis and AIM Analysis at Bond Critical Points. To estimate more precisely the character of proper hydrogen bonds, we have performed detailed NBO and topological analysis. The nature of the intermolecular hydrogen bonds has been analyzed within the framework of the NBO procedure. The NBO second-order perturbation energies of interaction are calculated as[41]

$$\Delta E_{ij}^{(2)} = 2\frac{|(\phi_i|F|\phi_j)|_2}{\epsilon_i - \epsilon_j}$$

where ϕ_i is the donor molecular orbital, ϕ_j is the acceptor molecular orbital, ϵ_i and ϵ_j are their energy eigenvalues, and F is the Fockian matrix element. $\Delta E_{ij}^{(2)}$ measures the strength of the donor−acceptor interaction between orbitals ϕ_i and ϕ_j and appears to be well suited to examining hydrogen-bond and other binding interactions. In all of the considered cases of binding,

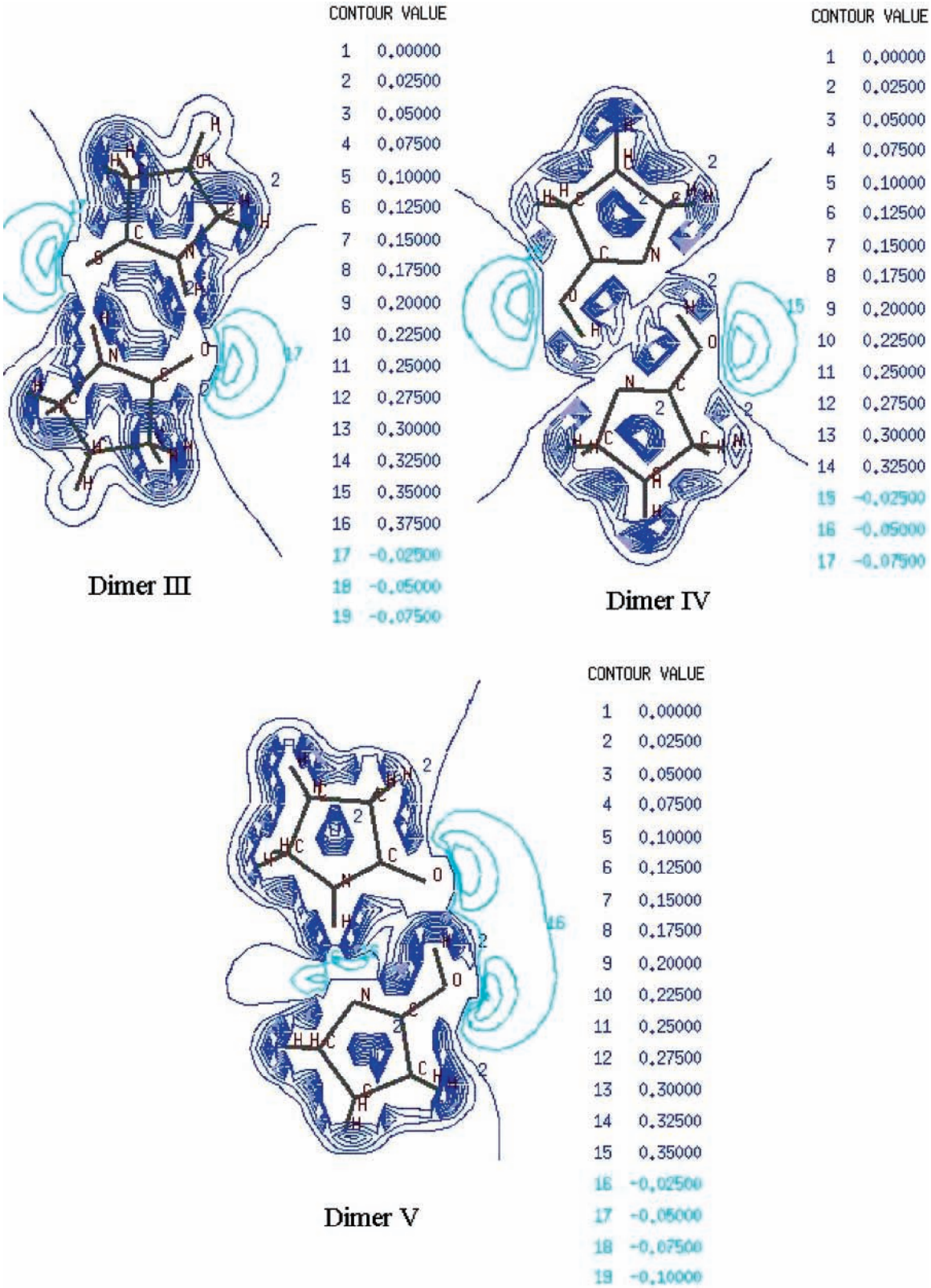

Figure 5. Contour map of true electrostatic potential for dimers **III**−**V** at B3LYP/6-311++G(d,p). The contour values are presented in Hartree/*e* (atomic energy unit per electron charge).

σ^*_{X-H} antibonds participate as electron acceptors, and n_Y lone pairs participate as electron donors in the intermolecular charge transfer so that the stabilization energies are high (Table 7).

The analysis of Table 7 shows that dimer **III** possesses two equivalent strong hydrogen bonds, and their second-order perturbation energies for interaction are 10.83 kcal/mol. The NBO results for dimer **IV** are indicative of a strong hydrogen bond with the second-order perturbation energy for interaction of 51.63 kcal/mol, and dimer **V** is characterized by two intermolecular interactions: $n_O \rightarrow \sigma^*_{O-H}$ (23.00 kcal/mol) and $n_N \rightarrow \sigma^*_{N-H}$ (19.37 kcal/mol). Obviously, the hydrogen bond in **IV** is stronger than that in **III** and **V**. There are miniscule charge transfers in the reverse direction. It should be noted that the recombination potentialities of the monomeric units in dimer

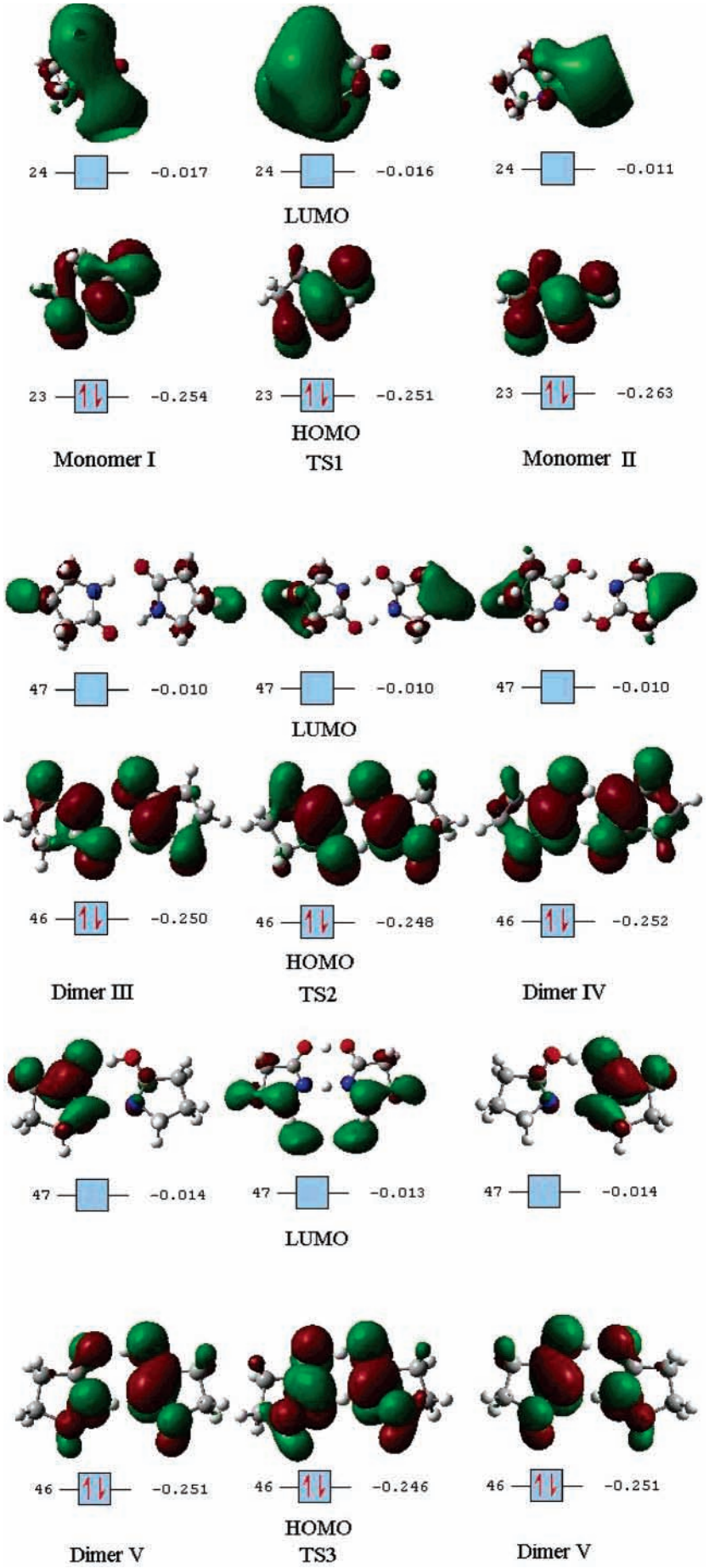

Figure 6. Schematic diagram of molecular orbitals with absolute orbital energies (au) for B3LYP/6-311++G(d,p) computations.

TABLE 7: B3LYP/6-311++G(d,p) NBO Analysis of Complexes III−V in the Gaseous Phase: Occupation Numbers for the σ^*_{X-H} Antibonds[a]

	σ^*_{O6-H14}	σ^*_{N8-H14}	σ^*_{N2-H7}	$\sigma^*_{O13-H14}$	$\phi_i \rightarrow \phi_j^*$	$\Delta E_{ij}^{(2)}$	ΔE_{DEL}
dimer **III**					LP (σ) O6 → BD* (σ) N8−H14	4.87	(1* → 2* and 2 → 1)
		0.051			LP (π) O6 → BD* (σ) N8−H14	10.83	38.260
		(0.018)			LP (σ) N8 → RY* O6	0.10	(1 → 2)
							19.269
dimer **IV**					LP (σ) N8 → BD* (σ) 06-H14	51.63	(1 → 2 and 2 → 1)
	0.123				BD(σ) O6−H14 → RY* N8	0.13	117.299
	(0.011)						(1 → 2)
							62.937
dimer **V**					LP (σ) O6 → BD* (σ) O13−H14	6.92	(1 → 2 and 2 → 1)
			0.064	0.071	LP (π) O6 → BD* (σ) O13−H14	23.00	59.027
			(0.018)	(0.011)	BD (σ) O13−H14 → RY*O6	0.07	(1 → 2)
					LP (σ) N8 → BD* (σ) N2−H7	19.37	24.997
					BD (σ) N2−H7 → RY* N8	0.21	(2 → 1)
							34.649

[a] The same parameters calculated for the isolated monomers are given in parentheses. The second-order perturbation energies $\Delta E_{ij}^{(2)}$ and the energy changes ΔE_{DEL} from the NBO energetic deletion analysis are given in kcal/mol. 1* → 2*, numbers of the monomeric units in dimers **III**−**V**.

IV are put in practice effectively and lead to strong interactions, that is, to the cooperative effect. Furthermore, in dimers **III** and **V** the charge transfer from the π orbital to the antibonding σ^*_{O-H} orbital occurs for dimers. The n(π) → σ^* interaction in **III** and **V** is much stronger compared to n(σ) → σ^*. Such results allow one to conclude the predominating π-type hydrogen-bonding interaction in dimers **III** and **V**.

In complexes **III** and **IV**, the charge density transfer to the X−H antibonding orbitals is greater compared to the corresponding monomers, which leads to the elongation of X−H bonds followed by a downshift of stretching vibrational frequencies (as we considered above). When the NBO results for isolated compounds are compared, it can be seen that in the dimers the σ^*_{X-H} antibond occupation numbers are higher compared to the isolated compounds (particularly for the σ^*_{O-H} antibond for dimer **IV**).

We have proceeded further with the NBO energetic deletion analysis.[39] Standard NBO energetic deletion analysis is performed by deleting specified elements from the NBO Fock matrix, diagonalizing this new Fock matrix to obtain a new density matrix, and passing this density matrix to the SCF routines for a single pass through the SCF energy evaluator. The difference between the energy obtained by such a "deletion" procedure and the energy obtained from starting density matrix is a good estimation of the total energy contribution of the deleted terms. Using this approach, we have removed all Fock matrix elements between the high-occupancy NBOs of the donor monomeric unit and the low-occupancy NBOs of the acceptor monomeric unit. That corresponds to total removal of the effects of intermolecular delocalization between monomeric units 1 and 2 in the studied dimer (both 1 → 2 and 2 → 1). The results are summarized in Table 7. The strongest effect of the above delocalizations is observed for dimer **IV**. Of course, the speculations and conclusions presented here about the degree of intermolecular delocalization are not to be taken in absolute quantitative terms. They are valuable only in the course of estimating the relative contributions to the total energy of intermolecular delocalizations and not of the overall contribution to the total interaction energy. This is so because, first of all, a single SCF step through which the new density matrix is passed does not lead to a full SCF convergence.

As a whole, the results of NBO analysis indicate that the intermolecular interactions in dimer **IV** are stronger than those in **III** and **V**.

To compare the default NBO Lewis structure with the alternative Lewis "resonance" structures chosen by user, we have used $CHOOSE keyword. In the $CHOOSE list, a resonance structure is specified by indicating where lone pairs and bonds are in the molecule. The non-Lewis occupancy of the $CHOOSE structure can be compared to the default NBO structure in order to assess the relative accuracy of the two descriptions. Thus, the use of $CHOOSE keyword enables one to prove a proper choice of the "true" best Lewis structure by the program. In accordance with the aforesaid, we have composed a series of Lewis structures for dimers **III**−**V**. The outcomes are presented in Table 8. As can be seen, the non-Lewis occupancies for Lewis structures 2−6 (dimer **IV**) are much more imperfect than those for the default structure, 1. These results confirm that the optimal NBO Lewis structure, 1, obtained in the course of NBO search without $CHOOSE is acceptable for dimers **III**−**V** and our NBO analysis results described above are realistic.

The AIM methodology has been used widely in the study of H-bonded systems and proved to be a useful and successful tool for interpreting charge density. To gain information on the hydrogen-bond strength in the above, we undertook the AIM study of electron density at bond critical points.

Several studies demonstrated the formation of hydrogen bonds to be associated with the appearance of a bond critical point between the hydrogen atom and the proton acceptor atom, which are linked by the bond path.[54−57] This critical point has typical properties of a closed-shell interaction: the value of electron density at the bond critical point, ρ_b, is relatively low, and the electron density Laplacian $\nabla^2\rho_b$ is positive, which points to a depletion of electron density from the interatomic basin toward the interacting nuclei.

Table 9 contains the data on electron density at the H-bond critical points as well as the data for the N−H and O−H bonds in the monomers and dimers. Contour maps of the Laplacian distribution for dimers **III**−**V** are displayed in Figure 7. As seen from Table 9 and Figure 7, the aforesaid conditions related to hydrogen bond formation are fulfilled at the Y···H (Y = N, O) bond critical points of complexes **III**−**V**. The N···H and O···H bond critical points are located in the regions of charge depletion (region of positive $\nabla^2\rho$ values). The electron densities at the Y···H bond critical points range from 0.031 to 0.070 au, which is in good agreement with the values reported for various hydrogen-bonded complexes.[56,57] Similarly, the Laplacian of the electron density ranges from 0.084 to 0.102 au, which is also reasonably comparable to the literature.[56,57] The increase in ρ_b values at the H-bond critical points results in H-bond strengthening. According to the actual ρ_b and $\nabla^2\rho_b$ values at the intermolecular bond critical points, applying the AIM-based

TABLE 8: Lewis and Non-Lewis Occupancies of Various "Resonance" Structures 1−6 in Terms of the Percentage (%) of the Total Electron Density

dimer **III**	1 (default)[a]	2 (lone pairs on both oxygens)	3 (lone pairs on both nitrogens)	4 (lone pairs on both oxygens and nitrogens)	5 (without lone pairs)	6 (without lone pairs)[b]
total Lewis	98.388	98.380	98.380	98.380	98.380	93.824
total non-Lewis	1.612	1.620	1.620	1.620	1.620	6.176
dimer **IV**	1 (default)[a]	2 (lone pairs on both oxygens)	3 (lone pairs on both nitrogens)	4 (lone pairs on both oxygens and nitrogens)	5 (without lone pairs)	6 (without lone pairs)[b]
total Lewis	98.481	92.906	92.789	92.906	92.789	94.257
total non-Lewis	1.519	7.094	7.211	7.094	7.211	5.743
dimer **V**	1 (default)[a]	2 (lone pairs on O6 and N8)	3 (lone pairs on O13 and N2)	4 (lone pairs on both oxygens and nitrogens)	5 (without lone pairs)	6 (without lone pairs)[b]
total Lewis	98.484	97.159	97.162	97.159	97.162	95.230
total non-Lewis	1.516	2.841	2.838	2.841	2.838	4.770

[a] Without $CHOOSE keyword. [b] All of the intermolecular hydrogen bonds are treated as trivial chemical bonds.

TABLE 9: Selected Properties of Bond Critical Points[a] (au) for 2-Pyrrolidone Monomers and Dimers in the Gaseous Phase at the B3LYP/6-311++G(d,p) Theory Level

	monomer **I**		monomer **II**		dimer **III**		dimer **IV**		dimer **V**	
bond	ρ_b	$\nabla^2\rho_b$	ρ_b	$\nabla^2\rho_b$	ρ_b; $\Delta\rho_b$	$\nabla^2\rho_b$; $\Delta(\nabla^2\rho_b)$	ρ_b; $\Delta\rho_b$	$\nabla^2\rho_b$; $\Delta(\nabla^2\rho_b)$	ρ_b; $\Delta\rho_b$	$\nabla^2\rho_b$; $\Delta(\nabla^2\rho_b)$
C1−O6	0.409	−0.258			0.394; −0.015	−0.335; −0.077			0.390; −0.019	−0.342; −0.084
N2−H7	0.338	−1.623			0.321; −0.017	−1.661; −0.038			0.314; −0.024	−1.624; −0.001
O6−H7			0.360	−2.510			0.284; −0.076	−1.776; 0.734		
O13−H14									0.317; −0.043	−2.188; 0.322
O6···H14					0.033	0.102			0.049	0.136
H7···N8							0.070	0.091	0.031	0.084

[a] ρ_b is the electron density value at the bond critical point; $\nabla^2\rho_b$ is the second-order derivative of the electron density (density Laplacian); $\Delta\rho_b = \rho_b^{complex} - \rho_b^{monomer}$ (complex = dimer **III**, **IV**, or **V**); $\Delta(\nabla^2\rho_b) = \nabla^2\rho_b^{complex} - \nabla^2\rho_b^{monomer}$ (complex = dimer **III**, **IV**, or **V**).

criteria of hydrogen bonding,[58] the hydrogen bonds under discussion may be arranged as the rather strong ones.

The X−H bond strength is also estimated by a comparison of the ρ_b and $\nabla^2\rho_b$ values, which correspond to the X−H BCPs in the case of free 2-pyrrolidone and its dimers (the BCP corresponds to the shared X−H interaction, i.e., the value of electron density at the bond critical point is relatively large and the Laplacian of the charge density is negative, indicating that the electronic charge is concentrated in the internuclear region). Figure 7 just shows that the X−H bond critical points occur in the regions of charge concentration (region of negative $\nabla^2\rho$ values). The ρ_b and $|\nabla^2\rho_b|$ values at the X−H BCPs decrease upon hydrogen bonding (Table 9), which points to X−H bond weakening in dimers compared to monomers.

The AIM analysis showed that the values of ρ_b and $\nabla^2\rho_b$ at the Y···H bond critical points increase when going from dimer **III** to **V** (Table 9). The increments are consistent with the intermolecular distance changes discussed above. Figure 8 illustrates the relief maps of the Laplacian distribution for all three dimers involved in this study. The oxygen atom in each dimer shows itself as a torus of charge concentration (which appears as four maxima). The nitrogen atom exhibits four quantum shells twice smaller in size than those for the oxygen.

It is interesting to compare the electron density properties of heteronuclear O···H−N and N···H−O bonds in dimers **III** and **IV**. It was shown recently that ρ_b(X···H−A) and $\Delta\rho_b$(H−A) reflect relatively small changes that may characterize the intermolecular H-bonding strength, and they are comparable quantities for different H-bond types.[58] The ρ_b(O···H), ρ_b(N···H), $\Delta\rho_b$(N−H), and $\Delta\rho_b$(O−H) values in dimers **III** and **IV** confirm the supposition that the N···H hydrogen bond is stronger compared to that of O···H.

Similarly, the data on homonuclear O···H−O and N···H−N bonding for dimer **V** indicate that the O···H bond surpasses the N···H one in strength.

In this study, we have established the correlation between the Y···H distances and electron densities at the corresponding bond critical points in dimers **III**−**V** according to the B3LYP/6-311++G(d,p) data. The linear regression plot is shown in Figure 9. One could observe that the electron density between the hydrogen atom and the proton acceptor decreases practically linearly with the increase in the Y···H distance. In addition, we have found the correlation of interaction energies of the studied complexes with the electron densities at the bond critical points (Figure 10). Linear regression analyses on the above correlations were performed using Microsoft Excel 2000 for Windows. The correlation coefficients (r) were −0.9468 (the Y···H distances against the electron densities at BCPs) and 0.9145 (the interaction energies against the electron densities at the BCPs).

To improve the latter correlation, we have removed the point corresponding to the N···H intermolecular bond of dimer **V** (a weaker interaction compared to the O···H one). As a result, the r value grew up to 0.9779 (Figure 11). For the number of points equal to three, the correlation coefficient's deviation from zero is significant in the only case of its strict equality to unity. However, the sufficiently high r value attests to the fact that the correlation obtained does not have a random nature.

The above correlations demonstrate the interrelation of topological, spatial, and energetic characteristics. Hence, Bader's

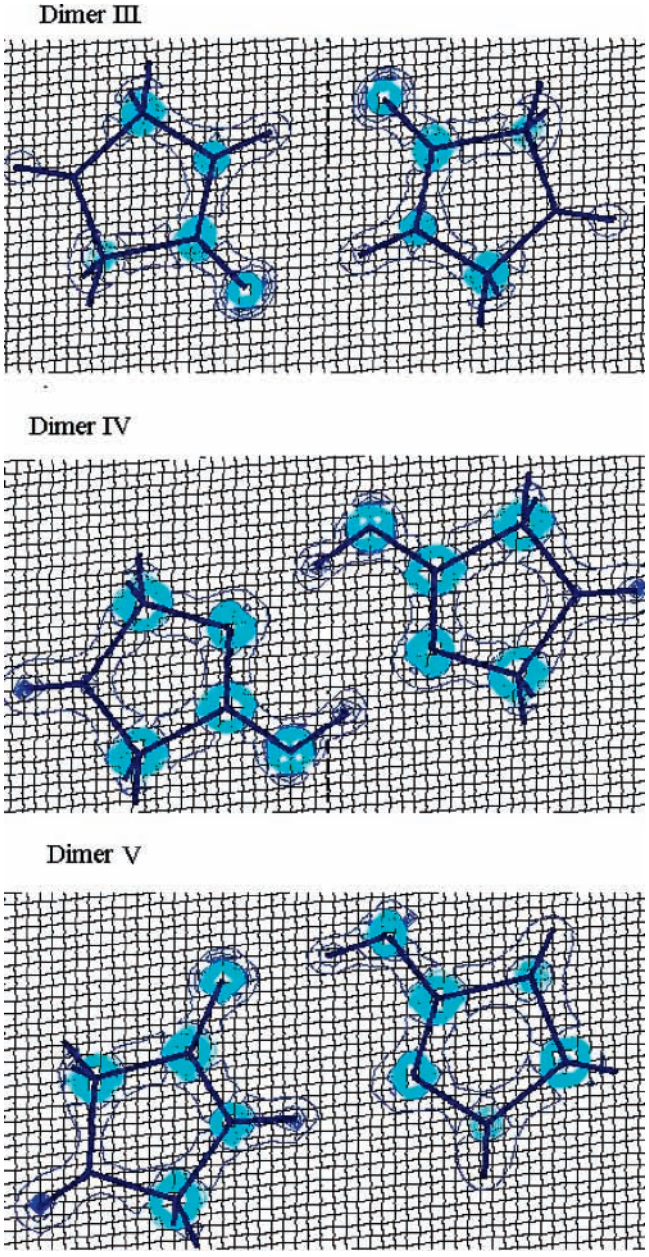

Figure 7. Contour maps of Laplacian distribution for dimers **III**−**V** at B3LYP/6-311++G(d,p). The solid contour zones and lines correspond to negative $\nabla^2\rho$ values.

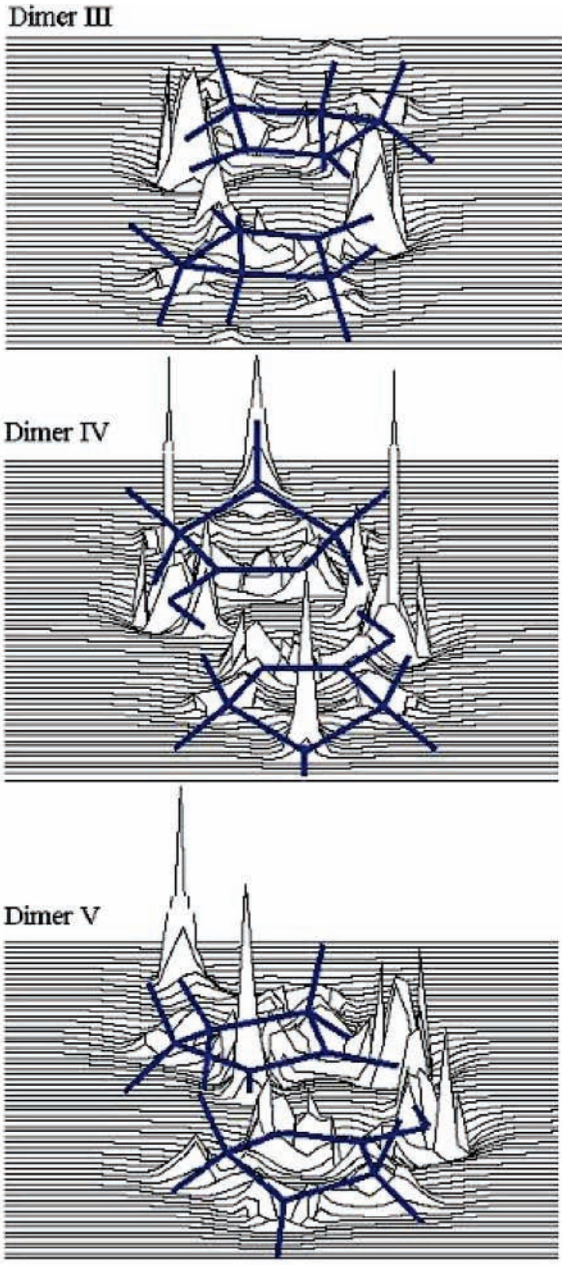

Figure 8. Relief maps of electron density Laplacian ($\nabla^2\rho$) for mean planes (center graph = center molecule) of dimers **III**−**V** molecules at B3LYP/6-311++G(d,p).

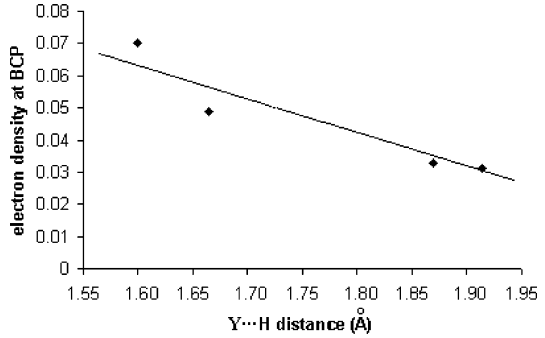

Figure 9. Correlation of Y···H distances in dimers **III**−**V** with electron densities at bond critical points (B3LYP/6-311++G(d,p)).

topological theory may be useful for evaluating the H-bonding interactions starting from the electron density, and the properties of the BCPs are useful descriptors for estimating the strength of intermolecular H-bonds.

Thus, the basic features of the donor−acceptor interaction when forming the 2-pyrrolidone dimers are reflected adequately by means of the reactivity indices describing both the charge-controlled[52] (charges on atoms, electrostatic potential) and orbital-controlled[52] (topology and energies of frontier orbitals, second-order perturbation energy for interaction) reactions. More delicate analysis of such interaction requires the approaches comprising the concepts on the charge-controlled and orbital-controlled reactions and exceeding the bounds of these concepts (NBO, AIM, etc.).

3.7. Interaction Energies. The interaction energies of the hydrogen-bonded dimers of 2-pyrrolidone were computed by means of different DFT methods using the 6-311++G(d,p) basis set. The uncorrected and corrected (with the allowance for BSSE and ZPVE quantities) hydrogen-bonding energies of dimers **III**−**V** are collected in Table 10. All of the methods predict the similar H-bonding interaction energies for each of the studied dimers, provided that the BSSE and ZPVE corrections are taken

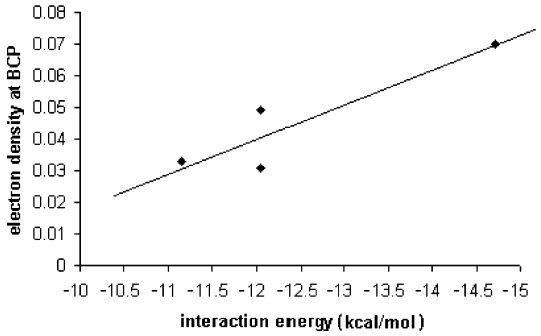

Figure 10. Correlation of interaction energies in dimers **III**−**V** (Table 10) with electron densities at bond critical points (B3LYP/6-311++G-(d,p)).

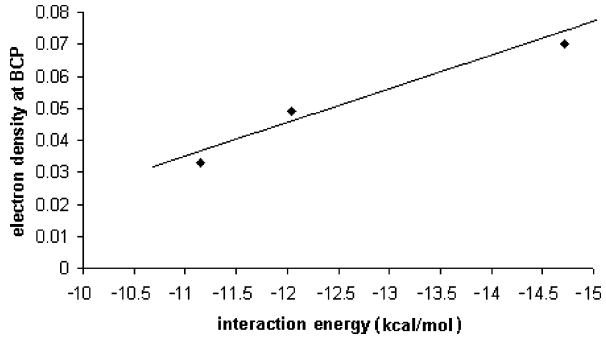

Figure 11. Correlation of interaction energies in dimers **III**−**V** (Table 10) with electron densities at bond critical points (B3LYP/6-311++G-(d,p)). The N···H hydrogen bond is excluded for dimer **V**.

TABLE 10: Interaction Energies (6-311++G(d,p), kcal/mol) for Various 2-Pyrrolidone Dimers[a]

		ΔE	BSSE	ΔE (BSSE)	ΔE $(BSSE)_{ZPVE}$	E^{exptl}
	B3LYP	−14.000	0.684	−13.316	−11.148	−7.6
dimer **III**	MPW1K	−14.943	0.550	−14.393	−12.246	
	B3PW91	−13.492	0.725	−12.767	−10.680	
	B3LYP	−22.037	6.342	−15.695	−14.717	
dimer **IV**	MPW1K	−23.878	6.373	−17.505	−16.534	
	B3PW91	−23.114	6.592	−16.522	−16.807	
	B3LYP	−15.856	1.896	−13.960	−12.047	
dimer **V**	MPW1K	−17.142	1.865	−15.277	−13.398	
	B3PW91	−15.817	2.314	−13.960	−11.746	

[a] See text for details and definitions.

into account. Because the N···O distance in dimer **IV** is shorter than this distance in dimer **III**, the interaction energy for dimer **IV** would be expected to be somewhat higher compared to dimers **III** and **V**. This can be seen in Table 10. Such a statement is substantiated by the enhanced charge-transfer interaction as well as by the strong intermolecular delocalization in dimer **IV** (Section 3.6, Table 7). In accordance with the aforesaid, the N···H bond (uniquely present in dimer **IV**, for which the interaction energy is the most negative) is stronger compared to the O···H bond occurring in dimers **III** and **V**.

A hydrogen-bonding energy of 7.6 kcal/mol has been determined experimentally for dimeric 2-pyrrolidone in CCl_4.[18] This agrees well with the value of 6.99 kcal/mol estimated for ϵ-caprolactam, which also forms centrosymmetrical hydrogen-bonded dimers in crystal.[18] As seen in Table 10, our computations overestimate the interaction energy for dimer **III** compared to the experimental data. The reason for that may be the following: the calculated N···O distance between the N and O atoms of different monomeric units (Table 1) is slightly shorter than the experimental one.

For dimers **III** and **V**, the BSSE values account for more than 5−11% of the total interaction energies, whereas for dimer **IV** this contribution is much more considerable at the same theory level.

To gain deeper insight into the intermolecular interactions binding the monomeric units in the 2-pyrrolidone dimers, we considered all types of hydrogen bonding. In the dimers, the following hydrogen bonds appear: O···N−H (dimer **III**), N···H−O (dimer **IV**), and N···H−N and O···N−H (dimer **V**). One can see in Table 10 that the most negative interaction energy was calculated for dimer **IV**. However, this bonding type was not observed in crystal.[18] The bonding type characteristic for dimer **III**, but not **IV**, has been just realized because the intrinsic stability of the monomeric units (Table 3) recovers the interaction energy contribution. Our results testify to the fact that **III** is energetically preferred.

4. Concluding Remarks

We have carried out the calculations using the B3LYP, MPW1K, and B3PW91 methods with 6-311++G(d,p) and AUG-cc-pVDZ basis sets in order to determine the equilibrium state and vibrational frequencies of the stable conformers for the monomers and dimers of 2-pyrrolidone. Two stable tautomers, **I** and **II**, for 2-pyrrolidone have been identified, and vibrational frequencies for species **I** are in good agreement with the earlier experimental data.

Among the three dimers of 2-pyrrolidone, **III** is the most stable both in vacuo and in aqueous medium. As has been ascertained, the intramolecular proton transfer in 2-pyrrolidone has a barrier of ∼50 kcal/mol, and this value does not depend substantially on solvation. The double proton transfer in the hydrogen-bonded dimers occurs concertedly and synchronously with a lower activation barrier. The **III** → **IV** reaction is a highly endothermic one, and the transition state is located near the reaction product. Great activation and relative energies imply that the reaction is kinetically and thermodynamically unfavorable in the gaseous phase and in aqueous solution, but the reverse process is kinetically and thermodynamically favored. The **V** → **V** double proton transfer reaction is kinetically and thermodynamically more preferable than **III** → **IV**.

For a proper hydrogen bond, the labile hydrogen-involving bond stretching frequency decreases on complexation, which is accompanied by the X−H bond elongation.[6,8] Because of the charge density increase on the antibonding orbital of the X−H bond and the electron density delocalization, the X−H bond lengthening and concomitant decrease in stretching vibrational frequency are observed, and, hence, the complexes under our study are proper hydrogen-bonded ones. The greater vibrational shift for the X−H bond and the more negative interaction energy for dimer **IV** compared to **III** and **V** provide additional evidence for the more profound cooperativity in structure **IV**. The interactions between the frontier orbitals lengthen the X−H bond and lower its vibrational frequency; thus, those may be a source of a red shift.

The analyses of the charge density, topological parameters, NBO, and interaction energies have shown that all of the systems studied in this paper satisfy the indicative criteria for hydrogen-bonding interactions. The NBO analysis has revealed the strong intermolecular interactions in those complexes, which lead to the charge transfer from the Y atom lone pairs to the σ^*(X−H) antibonds. As a consequence, the occupation numbers of these antibonds are fairly high. All of the results indicate that dimers **III**, **IV**, and **V** are hydrogen-bonded clusters, and the existence of π-type hydrogen bonding in **III** and **V** is proved by our

calculations. In general, the results of NBO and AIM analysis indicate that the intermolecular interactions in dimer **IV** are stronger than those in **III** and **V**. The results of this study also show that the topological parameters derived from Bader's AIM theory correlate well with the geometry and energetic parameters. The above properties may be useful descriptors for estimating the strength of intermolecular H bonds.

Acknowledgment. It is our great pleasure to thank Professor Frank A. Weinhold (University of Wisconsin-Madison) for helpful discussion regarding NBO analysis and Ph.D. Olga M. Tsivileva (Laboratory of Microbiology and Mycology, Institute of Biochemistry and Physiology of Plants and Microorganisms, Russian Academy of Sciences, Saratov, Russia) for valuable advice and discussion.

References and Notes

(1) Müller-Dethlefs, K.; Hobza, P. *Chem. Rev.* **2000**, *100*, 143−168.
(2) Lehn, J.-M. *Angew. Chem., Int. Ed. Engl.* **1990**, *29*, 1304−1319.
(3) Hobza, P.; Šponer, J. *Chem. Rev.* **1999**, *99*, 3247−3276.
(4) Šponer, J.; Hobza, P., *J. Am. Chem. Soc.* **1994**, *116*, 709−714.
(5) Aloisia, S.; Francisco, J. S. *Acc. Chem. Res.* **2000**, *33*, 825−830.
(6) Scheiner, S. *Hydrogen Bonding: A Theoretical Perspective*; Oxford University Press: Oxford, 1997.
(7) Hobza, P.; Havlas, Z. *Chem. Rev.* **2000**, *100*, 4253−4264.
(8) Hermansson, K. *J. Phys. Chem. A* **2002**, *106*, 4695−4702.
(9) Li, X.; Liu, L.; Schlegel, H. B. *J. Am. Chem. Soc.* **2002**, *124*, 9639−9647.
(10) Castro, M.; Salahub, D. R. *Phys. Rev. B* **1994**, *49*, 11842−11852.
(11) Li, Y.; Raeker, T. J.; Depristo, A. E. *Phys. Rev. B* **1994**, *50*, 14742−14745.
(12) Giugrea, C.-E. Pharmaceutical Lactams. [UCB SOC. An] Eng. Pat. Class A5B, (A61K) No. 1066887; Claimed 28.07.65; Published 26.04.67. Ref: Abstr. J. Chem., 1969, 8N444P.
(13) Trushina, E. V.; Labunskaya, V. I.; Shebaldova, A. D. *Koord. Khim.* **1991**, *17*, 1676−1679.
(14) Berezov, T. T.; Korovkin, B. F. *Hormones In Biological Chemistry* (in Russian); Moscow, **1998**; Chapter 8, pp 248−297.
(15) Walmsley, J. A.; Jacob, E. J.; Thompson, H. B. *J. Phys. Chem.* **1976**, *80*, 2745−2753.
(16) Walmsley, J. A. *J. Phys. Chem.* **1978**, *82*, 2031−2035.
(17) De Smet, K.; Kedziora, P.; Jadzyn, J.; Hellemans, L. *J. Phys. Chem.* **1996**, *100*, 7662−7668.
(18) Goddard, R.; Heineman, O.; Kruger, C.; Magdo, I.; Mark, F.; Schaffner, K. *Acta Crystallogr., Sect. C* **1998**, *54*, 501−504.
(19) Tupitsyn, I. F.; Shibaev, A. Y.; Kane, A. A. *Zh. Obshch. Khim.* **1985**, *55*, 135−144.
(20) Rigys, N. V. *Aust. J. Chem.* **1985**, *36*, 1585−1589.
(21) Banhegyi, G.; Angyan, J.; Kajtar, M. *Collect. Czech. Chem. Commun.* **1986**, *51*, 249−263.
(22) Peck, P. S.; McDermott, D. P. *Spectrochim. Acta, Part A* **1988**, *44*, 371−377.
(23) Cosentino, U.; Scolastico, C.; Moro, G.; Pitea, D. *J. Mol. Struct.: THEOCHEM* **1989**, *201*, 199−212.
(24) Pankratov, A. N.; Borodulin, V. B.; Chaplygina, O. A. *Koord. Khim.* **2005**, *31*, 523−529. Engl. Transl.: *Russian J. Coord. Chem.* **2005**, *31*, 494−500.
(25) Turi, L.; Dannenberg, J. J. *J. Am. Chem. Soc.* **1994**, *116*, 8714−8721.
(26) Frisch, M. J.; Trucks, G. W.; Schlegel, H. B.; Scuseria, G. E.; Robb, M. A.; Cheeseman, J. R.; Zakrzewski, V. G.; Montgomery, J. A., Jr.; Stratmann, R. E.; Burant, J. C.; Dapprich, S.; Millam, J. M.; Daniels, A. D.; Kudin, K. N.; Strain, M. C.; Farkas, O.; Tomasi, J.; Barone, V.; Cossi, M.; Cammi, R.; Mennucci, B.; Pomelli, C.; Adamo, C.; Clifford, S.; Ochterski, J.; Petersson, G. A.; Ayala, P. Y.; Cui, Q.; Morokuma, K.; Malick, D. K.; Rabuck, A. D.; Raghavachari, K.; Foresman, J. B.; Cioslowski, J.; Ortiz, J. V.; Stefanov, B. B.; Liu, G.; Liashenko, A.; Piskorz, P.; Komaromi, I.; Gomperts, R.; Martin, R. L.; Fox, D. J.; Keith, T.; Al-Laham, M. A.; Peng, C. Y.; Nanayakkara, A.; Gonzalez, C.; Challacombe, M.; Gill, P. M. W.; Johnson, B. G.; Chen, W.; Wong, M. W.; Andres, J. L.; Head-Gordon, M.; Replogle, E. S.; Pople, J. A. *Gaussian 98*, revision A.7; Gaussian, Inc.: Pittsburgh, PA, 1998.
(27) Becke, A. D. *J. Chem. Phys.* **1993**, *98*, 5648−5652.
(28) Lee, C.; Yang, W.; Parr, R. G. *Phys. Rev. B* **1988**, *37*, 785−789.
(29) Lynch, B. J.; Fast, P. L.; Harris, M.; Truhlar, D. G. *J. Phys. Chem.* **2000**, *A104*, 4811−4815.
(30) Perdew, J. P.; Burke, K.; Wang, Y. *Phys. Rev. B* **1996**, *54*, 16533−16539.
(31) Krishnan, R.; Binkley, J. S.; Seeger, R.; Pople, J. A. *J. Chem. Phys.* **1980**, *72*, 650−654.
(32) McLean, A. D.; Chandler, G. S. *J. Chem. Phys.* **1980**, *72*, 5639−5648.
(33) Kendall, R. A.; Dunning, T. H., Jr.; Harrison, R. J. *J. Chem. Phys.* **1992**, *96*, 6796−6806.
(34) Woon, D. E.; Dunning, T. H., Jr. *J. Chem. Phys.* **1993**, *98*, 1358−1371.
(35) Peng, C.; Schlegel, H. B. *Isr. J. Chem.* **1994**, *33*, 449−454.
(36) Schlegel, H. B. *Theor. Chim. Acta* **1984**, *66*, 333−340.
(37) Gonzalez, C.; Schlegel, H. B. *J. Phys. Chem.* **1990**, *94*, 5523−5527.
(38) Onsager, L. *J. Am. Chem. Soc.* **1936**, *58*, 1486-1493.
(39) Xantheas, S. S. *J. Chem. Phys.* **1996**, *104*, 8821−8824.
(40) Boys, S. F.; Bernardi, F. *Mol. Phys.* **1970**, *19*, 553−566.
(41) Glendening, E. D.; Reed, A. E.; Carpenter, J. E.; Weinhold, F. A. *NBO*, Version 3.1; 1995.
(42) Bader, R. F. W. *Atoms in Molecules: A Quantum Theory*; Clarendon Press: Oxford, 1990.
(43) Bader, R. F. W. *Chem. Rev.* **1991**, *91*, 893−928.
(44) Destexhe, A.; Smets, J.; Adamowicz, L.; Maes, G. *J. Phys. Chem.* **1994**, *98*, 1506−1514.
(45) Dimitrova, Y. *Spectrochim. Acta, Part A* **2001**, *57*, 2457−2462.
(46) 2-Pyrrolidinone, *National Institute of Standards and Technology Chemistry WebBook*; webbook.nist.gov/chemistry.
(47) Pankratov, A. N. *Zh. Anal. Khim.* **2005**, *60*, 149−156. Engl. Transl.: *J. Anal. Chem.* **2005**, *60*, 130−136.
(48) Shchavlev, A. E.; Pankratov, A. N.; Shalabay, A. V. *J. Phys. Chem. A* **2005**, *109*, 4137−4148.
(49) Steel, W. V.; Chirico, R. D.; Nguyen, A.; Hossenlopp, I. A. *AIChe Symp. Ser.* **1989**, *85*, 140−162.
(50) Lee, C. M.; Kumler, W. D. *J. Am. Chem. Soc.* **1961**, *83*, 4593−4596.
(51) Lynch, B. J.; Truhlar, D. G. *J. Phys. Chem. A* **2001**, *105*, 2936−2941.
(52) Klopman, G. *J. Am. Chem. Soc.* **1968**, *90*, 223−234.
(53) Rauk, A. *Orbital Interaction Theory of Organic Chemistry*, 2nd ed.; John Wiley & Sons: New York, 2001.
(54) Carroll, M. T.; Bader, R. F. W. *Mol. Phys.* **1988**, *65*, 695−722.
(55) Carroll, M. T.; Chang, C.; Bader, R. F. W. *Mol. Phys.* **1988**, *63*, 387−405.
(56) Popelier, P. L. A.; Bader, R. F. W. *Chem. Phys. Lett.* **1992**, *189*, 542−548.
(57) Koch, U.; Popelier, P. L. A. *J. Phys. Chem.* **1995**, *99*, 9747−9754.
(58) Platts, J. A. *Phys. Chem. Chem. Phys.* **2000**, *2*, 3115−3120.